Reply to Reviewer (1)'s comments on gmd-2016-150

We would like to thank the reviewer for further reading through this manuscript and the comments to improve this manuscript. Here are our responses.

Comments to author:

The authors have done some work to appropriately address my remarks and provide answers. The relevant discussion was also included at several places throughout the manuscript. I therefore recommend the manuscript be accepted for publication once the authors make the following typos that should still be considered.

L15: May delete 'efficient'.

Reply: Agreed.

L39: Consider using 'remote sensing of earth' instead of 'earth remote sensing'.

Reply: Accepted.

L51: May use [ ] instead of the outer ().

Reply: Agreed.

L66: May use 'various' or other words instead of 'all kinds of' ?

Reply: Agreed. The revised sentence is "…in diversified forms (Snyder and Zhang, 2003), have been widely developed in order to estimate the uncertainties of various problems in geophysical applications."

L118: Similar to the study (or implementation) in Mechri et al……

Reply: Corrected. The sentence is revised as "Similar to the study in Mechri et al…… ".

L125: May delete 'Explicitly'.

Reply: Accepted.

L136: The equation never happens in mathematic unless α is 1. May use another letter for the left Cb.

Reply: Corrected. We modified the equation as $C_b^i = \alpha \times C_b, \alpha = 50\%,55\%,...,150\%$.

L150: Eq.2 –> Eq. 3

Reply: Done.

L154: Move the definition of σ at L158 to this line.

Reply: Accepted.

L158: Is n at L137 the same as p at L158 ? If so, why not use the same letter, n or p ?

Reply: Corrected. We used n consistently in the revised manuscript.

L255: The sentence is too long. Rewrite it.

Reply: We re-organized the sentence as two separate sentences.

L297: Fig. 2 looks fine. However, cloud fraction and Normalized Jo are not the same thing. It may be better to consider Normalized Jo as Fig. 3.

Reply: Agreed. We modified Fig. 2c and Fig. 2d to be Fig. 3a and Fig. 3b. The following Figure captions are also corrected accordingly.

A method for retrieving clouds with satellite infrared radiances using the particle filter

Dongmei Xu[1,2] , Thomas Auligné[2], Gaël Descombes[2], and Chris Synder[2]

[1]*Key Laboratory of Meteorological Disaster, Ministry of Education (KLME) /Joint International Research Laboratory of Climate and Environment Change (ILCEC) /Collaborative Innovation Center on Forecast and Evaluation of Meteorological Disasters (CIC-FEMD), Nanjing University of Information Science & Technology, Nanjing 210044, China*

[2]*National Center for Atmospheric Research, Boulder, Colorado* 80301, *USA*

(2016/8/23)

* **Corresponding Author**

Dr. Dongmei Xu

Nanjing University of Information Science & Technology, College of Atmospheric science,

Ningliu road, No. 219, Nanjing, 210044, China

E-mail: xdmjolly@sina.com

Abstract

Ensemble-based techniques have been widely utilized in estimating uncertainties in various problems of interest in geophysical applications. A new cloud retrieval method is proposed based on the Particle Filter (PF) by using ensembles of cloud information in the framework of Gridpoint Statistical Interpolation system (GSI). The PF cloud retrieval method is compared with the Multivariate and Minimum Residual (MMR) method that was previously established and verified. Cloud retrieval experiments involving a variety of cloudy types are conducted with the PF and MMR methods respectively with measurements of Infrared radiances on multi-sensors onboard both geostationary and polar satellites. It is found that the retrieved cloud masks with both methods are consistent with other independent cloud products. MMR is prone to producing ambiguous small-fraction clouds, while PF detects clearer cloud signals, yielding closer heights of cloud top and cloud base to other references. More collections of small fraction particles are able to effectively estimate the semi-transparent high clouds. It is found that radiances with high spectral resolutions contribute to quantitative cloud top and cloud base retrievals. In addition, a different way of resolving the filtering problem over each model grid is tested to better aggregate the weights with all available sensors considered, which is proven to be less constrained by the ordering of sensors. Compared to the MMR method, the PF method is overall more computationally efficient, and the cost of the model grid-based PF method scales more directly with the number of computing nodes.

Keywords: cloud retrieval methods, particle filter, GSI system, cloud height

删除的内容: efficient

1. Introduction

Modern polar orbiting and geostationary airborne instruments provide researchers unprecedented opportunities for remote sensing of earth with continuous flows and almost complete spectral coverage of data. The primary cloud retrieval products from satellites are cloud mask (CM), cloud height (CH), effective cloud fraction (CF), and vertical structures of clouds with larger temporal and spatial scales. These cloud retrievals provide an immense and valuable combination for better initializing hydrometeors in numerical weather prediction (NWP), (Wu and Smith, 1992; Hu et al., 2006; Bayler et al., 2000; Auligné et al., 2011) regulating the radiation budget for the planet, and understanding the climate feedback mechanism (Rossow and Schiffer, 1991; Rossow et al., 1993; Brückner et al., 2014). Advanced cloud retrieval methods are able to retrieve clouds with multispectral techniques (Menzel et al., 1983; Platnick et al., 2003), among which the minimization methods usually directly utilize the difference between the modeled clear sky and the observed cloudy Infrared (IR) radiances [e. g., the minimum residual method, (Eyre and Menzel, 1989); the Minimum Local Emissivity Variance method, (Huang et al., 2004); and the Multivariate Minimum Residual method, (Auligné, 2014a)]. Specially, the Multivariate Minimum Residual (MMR) method is retrieving three dimensional multi-layer clouds by minimizing a cost function at each field-of-view (FOV) (Auligné, 2014b; Xu et al., 2015). MMR has been proven to be reliable in retrieving the quantitative three dimensional cloud fractions with Infrared radiances from

删除的内容: earth

删除的内容: (

删除的内容:)

multiple infrared instruments. However, MMR has limitations in several aspects due to its use of minimization for solution: 1) Part of the control variables accounting for the cloud fraction for some certain levels are under-observed since the channels are not sensitive to the existence of clouds for those heights. 2) When clouds at different heights show opacities with the same spectral signal, MMR could lose the ability to distinguish solutions involving clouds at those levels. 3) The computational cost for the minimization procedure in MMR is rather considerable.

Ensemble-based techniques, that usually reside in short-term ensemble forecasting (Berrocal et al., 2007), assembling existing model outputs (e. g., cloud retrievals) from varying algorithms (Zhao et al., 2012), or ensemble Kalman filter (EnKF) in diversified forms (Snyder and Zhang, 2003), have been widely developed in order to estimate the uncertainties of various problems in geophysical applications. To better account for the non-linearity between the observed radiance and the retrieval parameter, a novel prototype for detecting clouds and retrieving their vertical extension inspired by the particle filter (Snyder and Zhang, 2003; van Leeuwen, 2010; Shen and Tang, 2015) technique and Bayesian theory (Karlsson et al., 2015) is proposed in this study. As a competitive alternative for MMR, the PF retrieval method has same critical inputs required and cloud retrieval products as in MMR. A brief description of MMR and the new PF cloud retrieval algorithm are provided in the following section. Section 3 describes the background model, the data assimilation system, the radiative transfer models (RTMs), and the radiance observations applied in this study. Model configurations are also illustrated in section 3. In section 4, the

删除的内容: various

删除的内容: all kinds of

single test within one FOV is conducted before the performance of PF method is assessed by comparing its cloud retrievals with those from MMR and other operational cloud products. Section 4 also discusses the computational performance for the two methods. The conclusion and anticipated future work are outlined in section 5.

2. Methodology

Essentially, the PF cloud retrieval scheme retrieves clouds with the same critical inputs requested (i. e., clear sky radiance from the radiative transfer model and the observed radiance) and the same cloud retrievals as outputs (i. e., three dimensional cloud fractions, which is defined as the fraction of top of cloud as seen from a sensor) with the MMR method. Both cloud retrieval schemes consist of finding cloud fractions that allow best fit between the cloudy radiance from model and the observation. We use $c^1, c^2, ..., c^{\mathrm{K}}$ to denote the array of vertical effective cloud fractions for K model levels (c^1 for the surface and c^{K} for the model top) and c^0 as the fraction of clear sky with $0 \le c^k \le 1,\ \forall k \in [0, \mathrm{K}]$. The constraint for the cloud fraction is as follows,

$$\sum_{k=0}^{\mathrm{K}} c^k = 1 \tag{1}$$

In this study, a cloud on one model level with a given fraction c^k is assumed to block the radiation from its lower model levels. The radiation originating from its lower levels is assumed to contribute to the top of atmosphere radiance observed by

the satellites only with the residual fractions.

The MMR method is an approach to retrieve cloud fractions using the minimization technique. The residual of the modeled radiance and the observation is normalized by the observed radiance, which results in the following cost function, using c^k, $\forall k \in [0, \mathrm{K}]$ as the control variables,

$$J(c^0, c^1, c^2, ..., c^{\mathrm{K}}) = \frac{1}{2} \sum_{v} \left[\frac{R_v^{\mathrm{cloud}} - R_v^{\mathrm{obs}}}{R_v^{\mathrm{obs}}} \right]^2, \quad (2)$$

where $R_{\mathrm{v}}^{\mathrm{cloud}}$ is the modeled cloudy radiance, and R_v^{obs} the observed radiance at frequency v. This vertical cloud fraction $c^1, c^2, ..., c^{\mathrm{K}}$ and c^0 are control variables for the cost function, where the simulated R_v^{cloud} is defined as

$$R_v^{\mathrm{cloud}}(c^0, c^1, c^2, ..., c^{\mathrm{K}}) = c^0 R_v^0 + \sum_{k=1}^{\mathrm{K}} c^k R_v^k. \quad (3)$$

Here R_v^k is the radiance calculated assuming an overcast black cloud at the model level k and R_v^0 the radiance calculated in the clear sky. Both R_v^k and R_v^0 are calculated using a forward radiative transfer model with model profiles of temperature and moisture as inputs. Details of the schematic of the MMR method can be referred in (Xu et al., 2015; Descombes et al., 2014).

Particle filter (PF) approach is one of the nonlinear filters for data assimilation procedures to best estimate the initial state of a system or its parameters x_t, which describes the time evolution of the full probability density function $p(x_t)$ conditioned by the dynamics and the observations. Similar to the study in Mechri et al., 2014, the bibliography on PF focuses on estimating the parameters, which are cloud fractions c^k in Eq. (3), in this study. While MMR retrieves the cloud fractions on each model

删除的内容: (

删除的内容:)

vertical level by minimizing a cost function, PF calculates posterior weights for each ensemble member based on the observation likelihood given that member. In its simplest form, PF works by initializing a collection of cloud profiles as particles and then estimating the cloud distributions by averaging those particles with their corresponding weights. Each particle's weight is computed with the difference between the modeled cloudy radiance from the particle and the observed radiance.

删除的内容: Explicitly, e

As the probabilities of the cloud distribution are fully presented by the initial particles, of particular interest is to evaluate different particle initialization schemes in the PF method. Explicitly, the definition of particles corresponds with ensemble members, i.e. one cloud profile as one of particles is corresponding to an ensemble member.

Two approaches for generating particles are firstly designed; the first one is to generate the perturbed samples C_b^i ($\forall i \in [1,n]$) from the cloud profile in the background denoted as $C_b = (c_b^0, c_b^1, ..., c_b^K)$ by inflating (deflating) the clouds with small magnitudes ($C_b^i = \alpha \times C_b, \alpha = 50\%, 55\%, ..., 150\%$) and moving upward (downward) with $\delta z = +5, +4..., -1, ... -5$ as the vertical magnitude, where n is the sample size. The perturbed cloud fractions are designated to replenish the ensemble by introducing the prior information of the cloud distributions from the background and to increase the ensemble spread.

Besides those perturbed particles, to represent the existence of one-layer cloud on each model level with an even chance, another diversity set of profiles C_b^i ($\forall i \in [0,K]$) are also initialized, among which, C_b^i stands for the profile with 100%

143 cloud fraction on the model level i (c^i=100%) and 0% cloud on the rest levels. In
144 particular, C_b^0 defines 100% clear (c^0=1). It is also interesting to discretize the initial
145 particles by setting the one-layer cloud with the value of c^i from 100% to 0% (e. g.,
146 100%, 90%, 80%, …, 0% with 10% as the interval) and further from 100% to 0% (e.
147 g., 100%, 99%, 98%, 97%, …, 0% with 1% as the interval). In this cases, c^0=1-c^i . For
148 each particle C_b^i, its simulated cloudy radiance $R_{v,i}^{\text{cloud}}$ from the model background can
149 be obtained with Eq. (3).

150 A cost function J_o is defined for each particle to measure how the particle fit the
151 observation as,

152 $$J_o = \left(\frac{R_v^{\text{obs}} - R_{v,i}^{\text{cloud}}}{\sigma}\right)^2. \quad (4)$$

153 σ is the specified observation error, which can be referred in the first paragraph in
154 section 4.1. The weight w^i for each particle C_b^i thus is calculated by comparing the
155 simulated $R_{v,i}^{\text{cloud}}$ and the observation R_v^{obs} using the exponential function by
156 accumulating the J_o for multiple frequency as

157 $$w^i = e^{-\sum_v \left(\frac{R_v^{\text{obs}} - R_{v,i}^{\text{cloud}}}{\sigma}\right)^2}, \quad (5)$$

158 $\forall i \in [1, n]$. Here n is the particle size. The final analyzed C_a is obtained by averaging
159 the background particles C_b^i with their corresponding weight, as

160 $$C_a = \sum_{i=1}^{n} w^i C_b^i. \quad (6)$$

161 In Eq. (6), the constraint referred in Eq. (1) is not respected. Thus, after the analysis
162 step for the particle filter, the final averaged cloud fractions c_a^k are normalized by

删除的内容: 2

删除的内容: p

删除的内容: and σ is the specified observation error, which can be referred in the first paragraph in section 4.1

$$c_a^k = \frac{c^k}{\sum_{k=0}^{\mathrm{K}} c^k}, \tag{7}$$

where $\forall k \in [0, \mathrm{K}]$.

3. Data and model configurations

3.1 Data

The Advanced Infrared Sounder (AIRS), the Infrared Atmospheric Sounding Interferometer (IASI), and the Cross-track Infrared Sounder (CrIs) are among the most advanced hyperspectral infrared sounders and thus are applied for retrieving clouds with hundreds of channels (Blumstein et al., 2004) (Aumann et al., 2003; Xu et al., 2013; Smith et al., 2015). The Radiance measurements from Moderate Resolution Imaging Spectroradiometer (MODIS) onboard the Earth Observing System (EOS) Terra or Aqua satellites are also well suited to extracting valuable cloud information from the 36 spectral broadbands in the visible, near infrared and infrared regions at high spatial resolution (1–5 km) (Ackerman, 1998). Apart from the IR radiances from polar satellites, the Geostationary Operational Environmental Satellites (GOES) Imager (Menzel and Purdom, 1994) provides a continuous stream of data over the observing domain. In this study, GOES-13 (east) and GOES-15 (west) are also utilized to obtain cloud fractions over the continental United States (CONUS) domain. The GOES Imager used in this study is a five-channel (one visible, four infrared) imaging radiometer designed to sense radiant and solar

reflected energy. The instrument parameters for the sensors and the setups for channel selections can be found in (Xu et al., 2015).

3.2 WRF, GSI and the radiative transfer model

The background fields are processed running the Weather Research and Forecast (WRF) model (Skamarock et al., 2008). The MMR and PF cloud retrieval algorithms are both implemented based on the gridpoint statistical interpolation data assimilation system (GSI) (Wu et al., 2002; Kleist et al., 2009), which is a widely used data assimilation system in operations and researches in NWP. GSI is capable of ingesting a large variety of satellite radiance observations and has developed capabilities for data thinning, quality control, and satellite radiance bias correction. The Community Radiative Transfer Model (Liu and Weng, 2006; Han et al., 2006) was used as the radiance forward operator for computing the clear-sky radiance and the radiance given overcast clouds at each model level.

3.3 Model configurations

The WRF is configured with 415*325 horizontal grids at 15-km grid spacing, and 40 vertical levels up to 50 hPa within the single CONUS domain. The MMR and PF cloud detection schemes search the cloud top using approximately 150 hPa as the highest extent for most cloudy cases. Other clouds higher 150 hPa, e.g. an anvil cloud in a mature thunderstorm around tropopause at low latitude region will also be explored in future studies. Channels in the longwave region are utilized following the

channel selection scheme in (Xu et al., 2015). Since the final retrieval clouds are on model grids, the retrieved cloud fractions within one FOV are essentially extrapolated to its four neighboring model grid points. Generally, for each FOV, the retrieved cloud fractions are extrapolated to its four neighboring model grid points. For polar satellite pixels, the representative cloud fractions are extrapolated with an adaptive radius with respect to their scan positions. The cloud detecting procedure for retrieving clouds is conducted for each FOV from each individual sensor independently and sequentially. Since the clouds are retrieved FOV by FOV and the clouds on grids are referred immediately after one FOV is completed, there is no obvious accuracy loss of radiance observations using this conservative method.

4. Experiments and results

The PF experiments apply two groups of particles as mentioned in section 2, among which the group-2 particles contains solely 100% one-layer clouds. To reveal how the setup of the initial particles impacts the results, apart from the MMR and PF experiments, we included another advanced experiment, denoted as APF. APF requires more sampled particles including ranges of cloud fractions spanning from 0% to 100% at the interval of 10%. An additional experiment “APFg2”, similar to APF but excluding the perturbed particles from the background in group-1 introduced in section 2, was conducted to evaluate the added values from the group-one particles. In this section, cloud retrieval experiments for several cases containing clouds of a variety of types are conducted for comparison reason. The GOES imager retrieved

products from National Aeronautics and Space Administration (NASA-Langley cloud and radiation products) are applied as a reference to validate the cloud retrieving methods for the CONUS domain with a large and uniform coverage of cloud mask. In addition, the retrieved cloud products were also compared to available CloudSat (Stephens et al., 2002) and MODIS level-2 cloud products (Platnick et al., 2003) archived by the CloudSat Data Processing Center in Colorado State and NASA respectively.

4.1 Single test at one field of view

The PF cloud retrieving algorithm retrieves the cloud distributions by averaging those initial particles with their weights. Before the real case experiments are carried out over the whole domain, we conduct a single cloud retrieving test at one FOV to understand what differences can be explained by the differences in the basic initial particles. In Eq. (5), the observation error σ can be set proportional to the observation, equaling to $\frac{R_v^{\text{obs}}}{r}$, where r is the prescribed ratio. Thus, the cloud signals on each level k are virtually determined by the extent of how close the $\frac{R_v^k}{R_v^{\text{obs}}}$ (and $\frac{R_v^0}{R_v^{\text{obs}}}$ for the clear part) gets to 1. An example of the ratio of the overcast radiance and the observed radiance $\frac{R_v^k}{R_v^{obs}}$ for each model level is given in Fig. 1 of GOES-Imager for the channel 5 (~13.00 μm). The clear sky radiance normalized by the observed radiance $\frac{R_v^0}{R_v^{\text{obs}}}$ is also shown at the level 0 (Fig. 1). It is expected that

the overcast radiance from the RTM decrease with the rising of the altitude. The cloud signal is strongest around level 5, where R_v^k fits R_v^{obs} most closely. The cloud retrievals depend not only on the basic input profiles (i.e., the overcast radiance on each level from RTM normalized by the observed radiance and the clear sky radiance from RTM normalized by the observed radiance) and but also on the algorithm applied for resolving the problem (e.g., MMR and PF in this study).

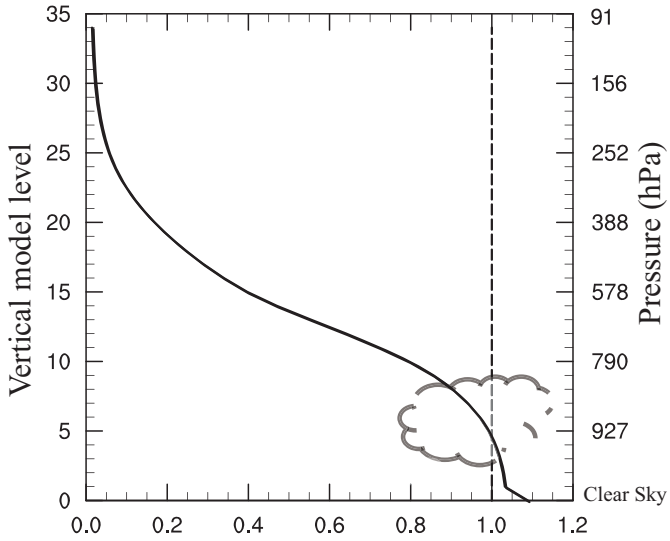

Figure 1. Ratio of the overcast radiances versus the observed radiance starting from the level 1. The ratio of the clear sky radiance normalized by the observed radiance corresponds to the level 0 (see text for explanation) for GOES-Imager for the channel 5. The approximate pressures corresponding to the model levels are also denoted.

To reveal the roles of various initial particles, Fig. 2a shows the weights for different particles on the given FOV for channel 5 of GOES-Imager for the case shown in Fig. 1. Particles in Fig. 1 include one-layer cloud in group 2 described in section 2 with specified value of cloud fractions c^k (on the x-axis) on specified model

删除的内容：of

levels k (on the y-axis) from 10% to 100% every 10%. With a fraction c^k of one-cloud layer at a given level k and a fraction of $c^0 = 1 - c^k$ of clear sky, the simulated cloudy radiance can be denoted as $R_v^{\text{cloud}} = c^k R_v^k + (1 - c^k) R_v^0$. Hence the theoretical one-layer cloud fraction is solved as $c^k = \frac{R_v^0 - R_v^{obs}}{R_v^0 - R_v^k}$ by fitting R_v^{cloud} to R_v^0. As expected, for one-layer cloud with full fraction, c^5 fits most closely to 100% . Since with the concept that $R_v^k > R_v^{k+1}$, no cloud can be present below level 5 since this would implies a R_v^{cloud} larger than the observation (or a c^i larger than 100%). It seems that clouds can be described by different possible states as particles with both large fractions and small fractions. Low clouds are easily estimated by one-layer cloud profile with large fractions (larger than 10%). The particles with small-fraction high clouds gain some weights to retrieve high clouds. The particle with the one-layer cloud on level 13 seems to gain least weight compared to the others levels. The weights for the particles with cloud fractions from 0% to 100% at the interval of 1% are also presented in Fig. 2b. By including more small-fraction one-layer clouds, the clouds around level 13 can be reproduced by the group of refined particles with 1% as the interval for approximate 10% cloud fractions. However, changing the level of the cloud for the fixed fraction (10%) does not seem to change the outgoing radiance much, probably due to the channel's low weight function peak (~750hPa).

The normalized J_o in Eq. (6) for different levels with a specific cloud fraction from 0% to 100% every 10% are shown in Fig. 3, with 10% and 1% as the intervals in Fig. 3a and Fig. 3b respectively. Here, J_o can be further derived as

删除的内容: on the given FOV for channel 5 of GOES-Imager for the case shown in Fig. 1

删除的内容: the bottom panel of

删除的内容: 2

删除的内容: 2c

删除的内容: 2d

$$J_o = r^2(1 - c^0 \frac{R_v^0}{R_v^{\text{obs}}} - c^k \frac{R_v^k}{R_v^{\text{obs}}})^2 \quad (8),$$

with $\sigma = \frac{R_v^{obs}}{r}$ and $R_v^{\text{cloud}}(c^0, c^1, c^2, ..., c^{\text{K}}) = c^0 R_v^0 + \sum_{k=1}^{\text{K}} c^k R_v^k$.

From Fig. 3a, it is found that J_o is smallest around level-5 with 100% cloud fraction (denoted as 1 in legend) for the thin black line, with respect to the fact that the overcast radiance fits the observed radiance most closely for level-5 approximately. The gray line with 10% cloud fraction (0.1 in the legend) corresponds to the existence of a weight peak on level 19 in Fig. 2a. In addition, the gap between the gray line with 0.1 and the other lines from 0.2 to 1 explains why there's less continuity around level 13. Fig. 3b shows a similar pattern to Fig. 3a, except with densely-distributed J_o values around the level 13 from 0.1 to 1 in the legend. Those contiguous black lines in Fig. 3b are associated with the set of particles with cloud fractions from 10% to 100% at the interval of 1%.

删除的内容: 2c

删除的内容: 2d

删除的内容: 2c

删除的内容: 2d

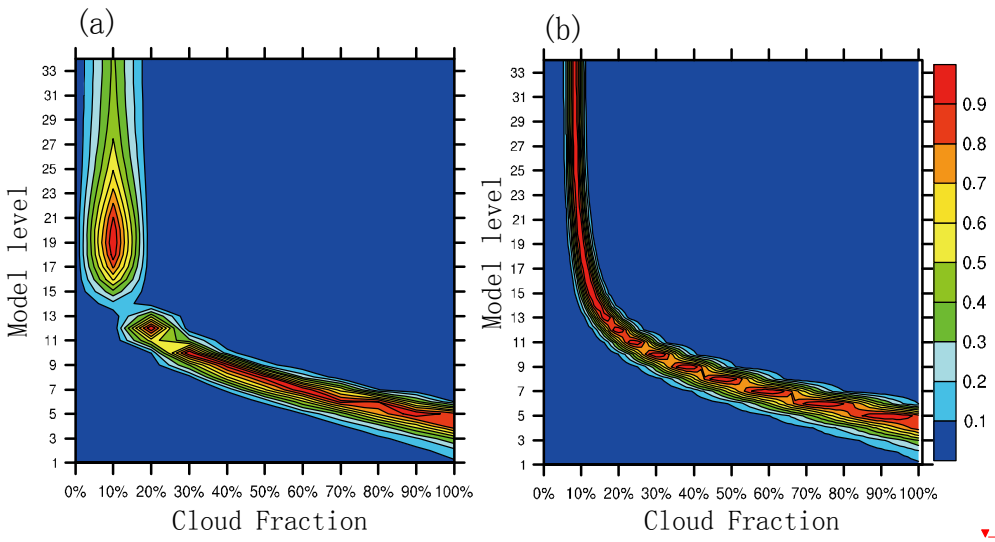

删除的内容:

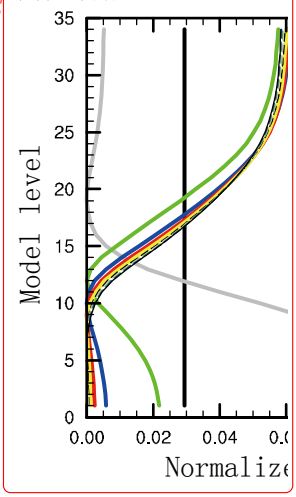

Figure 2. The weights for different particles with specified cloud fractions on the x-axis at one chosen model level shown on the y-axis from 0% to 100% (a) at the interval of 10% and (b) at the interval of 1%.

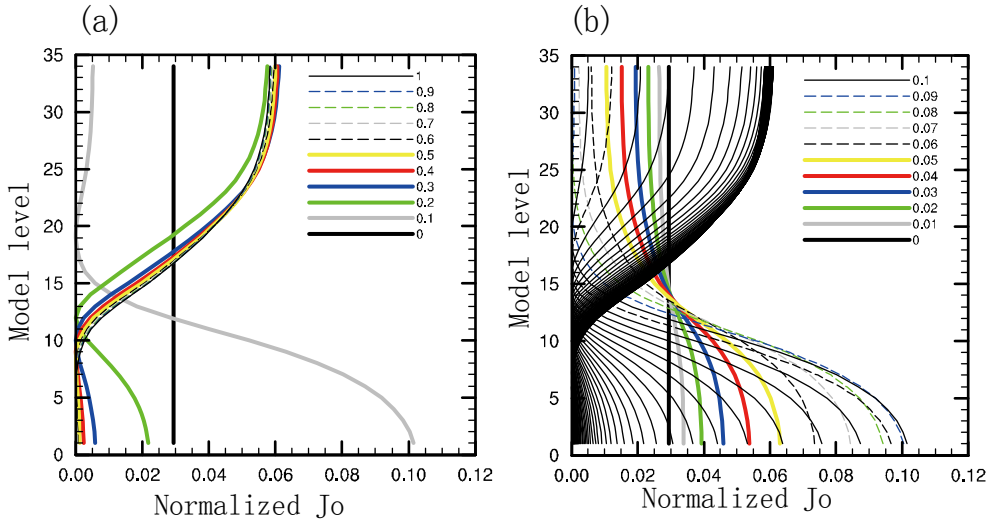

Figure 3. The normalized J_o (a) at the interval of 10% and (b) at the interval of 1%. In (b), the normalized J_o from 0.1 to 1 are all denoted as black lines.

删除的内容: c

删除的内容: d

删除的内容: d

4.2 Cloud profiles

The retrieval experiments for a real case are conducted at 1100 UTC 3 June 2012 when AIRS measurements and the CloudSat "2B-GEOPROF" products (Mace, 2004) are available. The vertical cross sections of the cloud fraction field of a real case are illustrated to further check how different collections of initial particles impact the retrieved cloud profiles. The standard radar reflectivity profiles from the CloudSat are shown in Fig. 4a as the validation source; Fig. 4b, Fig. 4c, and Fig. 4d show the cross sections of the cloud fractions along the CloudSat orbit tracks from the MMR, PF and APF experiments. The vertical structures of the clouds from MMR compare well with the radar reflectivity from CloudSat by retrieving the high clouds around 47N° and low clouds around 52N°. The PF experiment has difficulties in detecting the cloud tops appropriately. PF tends to detect a large quantity of low clouds; by adding a set of particles with small-fraction clouds in APF, higher clouds can be reproduced, which is consistent with the implications from Fig. 2b and 3b. APF detects clear strong cloud signals and removes the cloud fractions on near-surface levels around 36 N° successfully. Since the existences of ground-layer radar reflectivity are likely corresponding to the strong reflection from the underlying surface of the earth, the height of cloud bases of MMR and PF are not compared in this sub-section. The experiments with larger size of particles including 0% to 20% (at the interval of 1%) plus 30% to 100% (at the interval of 10%) or of 0% to 100% (at the interval of 1%) one-layer cloud profiles (introduced in section 2) yield similar results from APF but are much more costly (not shown).

删除的内容: 3

删除的内容: 3

删除的内容: 3

删除的内容: 3

删除的内容: 2d

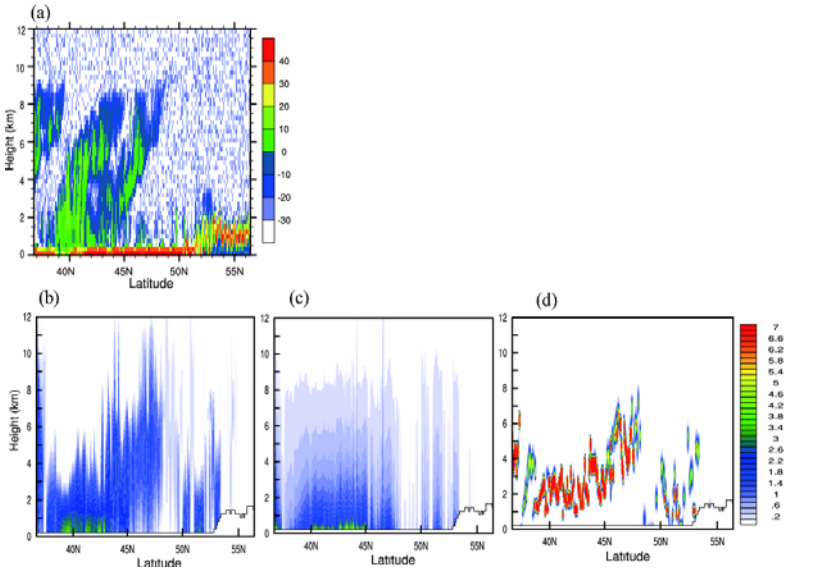

Figure 4. (a) The radar reflectivity (units: DBZ) cross sections from CloudSat, (b) the MMR retrieved cloud fractions (units: %) cross sections, (c) the PF retrieved cloud fractions, and (d) the APF retrieved cloud fractions valid at 1100 UTC 3 June 2012.

The vertical profiles of the averaged cloud fractions from MMR, PF, and APF are plotted in Fig. 5 at 1100 UTC 3 June 2012 with AIRS. Both MMR and PF experiments yield ambiguous cloud distributions, whereas APF retrieves much stronger cloud signals constrained between level-2 to level-20 (approximately from 950hPa to 400hPa). More clouds around level 10 are retrieved (approximately 750hPa) in MMR, while PF is prone to retrieving clouds near surface levels. Note that MMR retrieves much higher cloud tops and lower cloud bases compared to APF. The cloud base from PF is lowest; the cloud top from MMR and PF is comparable. Only the APF related methods will be further discussed in later sections owing to the missing of high clouds using PF.

删除的内容: 3

删除的内容: 4

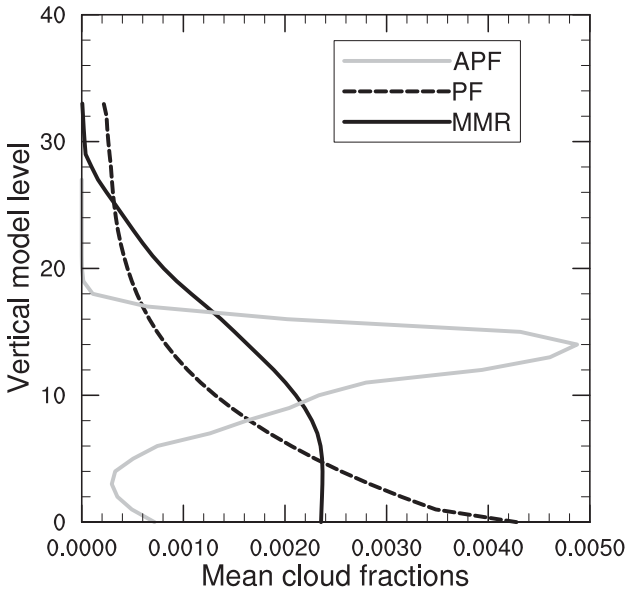

Figure 5. The mean cloud fraction on all model levels for the experiments MMR, PF, and APF with AIRS observations valid at 1100 UTC 3 June 2012.

删除的内容: 4

4.3 Cloud mask

Comparison experiments on real cases are further performed for over longer time period from 0000 UTC 12 December 2013 to 0700 UTC 12 December 2013. The cloud mask is marked as cloudy when there is a recognizable existence of cloud on any level from MMR or PF retrievals. Both the NASA GOES Imager products and the MMR-retrieved fields are interpolated to the same 0.1°×0.1° latitude–longitude grid with 0 for clear and 1 for cloudy before the comparisons for verification. Fig. 6 shows the *hits*, *false_alarms* and *misses* locations with the use of GOES-Imager, MODIS, CrIS, AIRS, and IASI radiances in the retrieval algorithms at 0700 UTC 12 December 2013. Note that, cloud mask retrievals from both the MMR and APF hit the clear and cloudy events well in Fig. 6a and 6b. In most areas, the MMR experiment

删除的内容: 5

删除的内容: 5

删除的内容: 5

overestimated the cloud mask with more false alarm events compared to the APF experiment, since the MMR solution is an “overly smoothed” estimation of the true vertical profile. It seems that the accuracy of cloud detection is lower for areas with high altitude than under tropical conditions, indicating that the smaller lapse rate in the atmosphere will lead radiance less sensitivity to clouds over polar areas. Fig. 6c shows the cloud mask results from the APFg2 experiment without the perturbed particles in group-1 introduced in section 2. There is no large discrepancy between Fig. 6b and Fig. 6c, suggesting that the particles in group-2 that fully span the possibility of the cloud distributions, are more determinant in retrieving the cloud mask.

删除的内容: 5

删除的内容: 5

删除的内容: 5

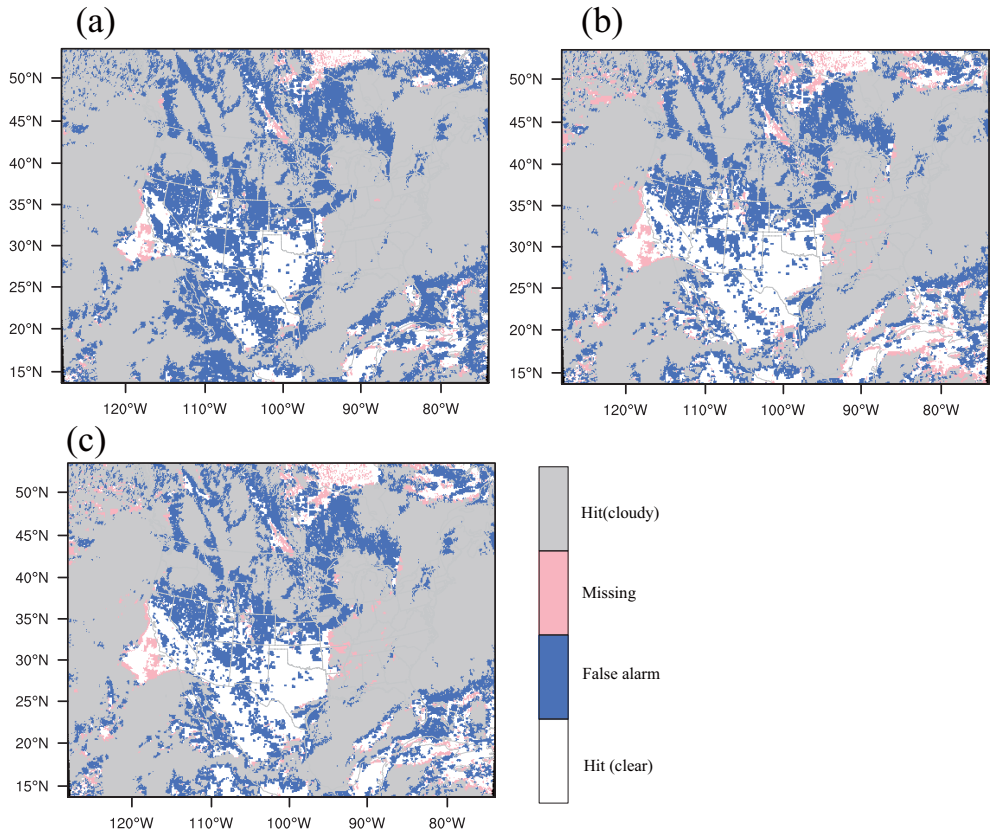

Figure 6. The false alarms, misses, and hits for clear and cloudy event locations with (a) the MMR method, (b) the APF method, and (c) the APF method but without the group-1 particles (see text for detailed explanations) valid at 0700 UTC 15 December 2013.

删除的内容: 5

4.4 Cloud top and base pressure

The retrieved cloud top pressures (CTP) and cloud bottom pressures (CBP) from this study along with the NASA GOES cloud products are illustrated in Fig. 7. The CTPs from both methods are in good accordance with the NASA cloud products for high clouds (from 100 hPa to 600 hPa) in Fig. 7a, 7c, and 7e. The retrieved cloud top heights from MMR are overall higher than those from the NASA reference, especially for lower clouds at approximately 750-1000 hPa (e. g., between longitude -100° and -90°). On the other hand, the CTPs from APF are much closer to those in the reference for both high and low clouds. APF overestimates the CBPs for some low clouds (putting the clouds too low) in Fig. 7f; the overestimation of the CBP is even more obvious from MMR in most regions in Fig. 7d.

删除的内容: 6

删除的内容: 6

删除的内容: 6

删除的内容: 6

删除的内容: 6

删除的内容: 6

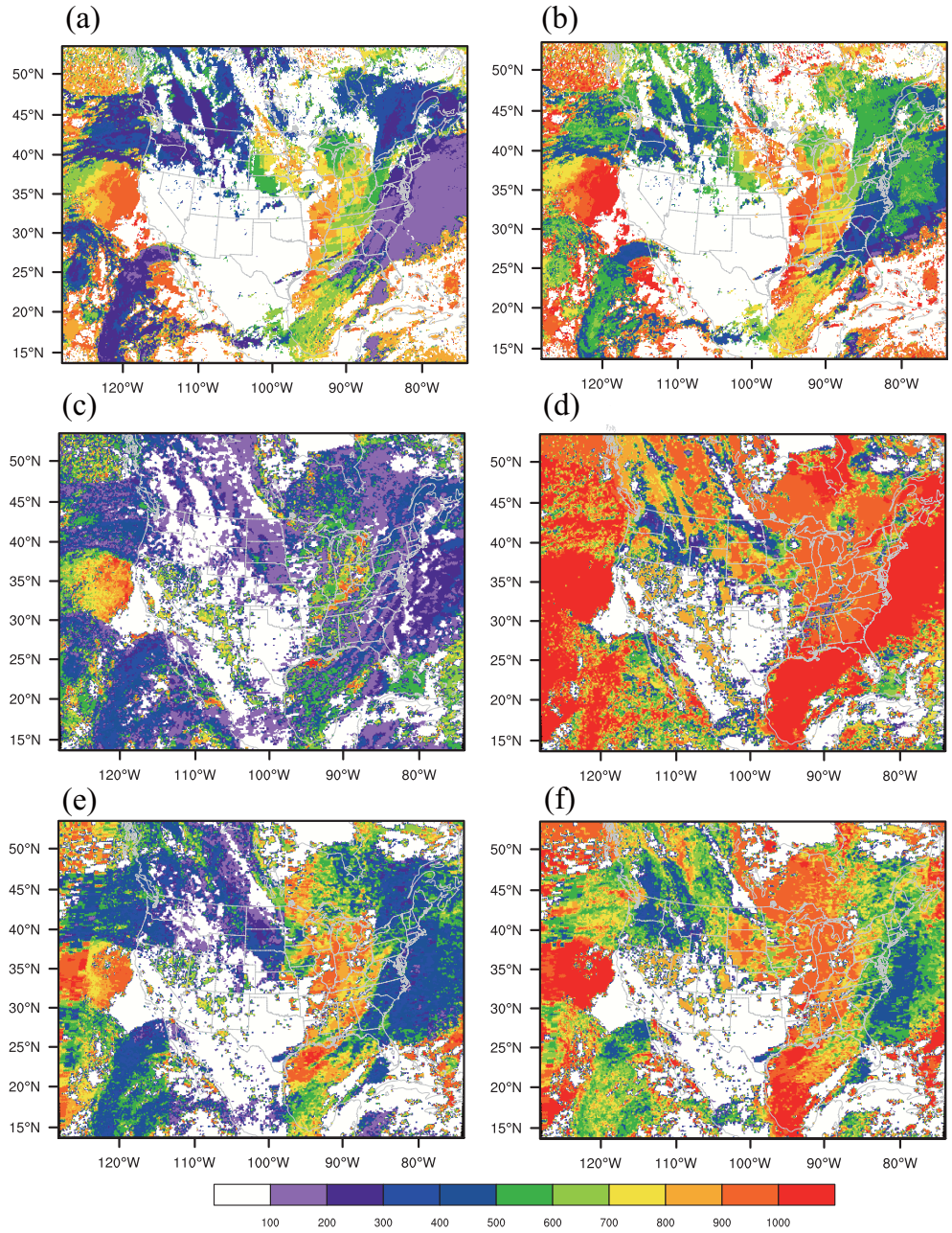

删除的内容: 6

Figure 7. The cloud top pressure (left panels) from (a) the NASA GOES retrieval, (c) the MMR method, (e) the APF method, and the cloud bottom pressure (right panels) from (b) the NASA GOES retrieval, (d) the MMR method, (f) the APF method valid at 0700 UTC 15 December 2013.

The CTPs from NASA GOES cloud products for more hours (0300UTC, 0500UTC, 0700UTC) together with the independent CTP retrievals from MODIS

level-2 products (http://modis-atmos.gsfc.nasa.gov/MOD06_L2/) are plotted in Fig. 8. Different sub-periods of the MODIS cloud retrieval products (e.g., Fig. 8b valid at 0320 UTC, Fig. 8c at 0325, and Fig. 8d at 0330 UTC) are chosen to approach the valid times in Fig. 8a, Fig. 8e, and Fig. 8h respectively. The CTPs from both cloud products agree well for both high and low clouds, confirming that NASA GOES cloud products are overall reliable for verifying the cloud retrievals and MODIS level-2 products can also be applied for validations.

删除的内容: 7

删除的内容: 7

删除的内容: 7

删除的内容: 7

删除的内容: 7

删除的内容: 7

删除的内容: 7

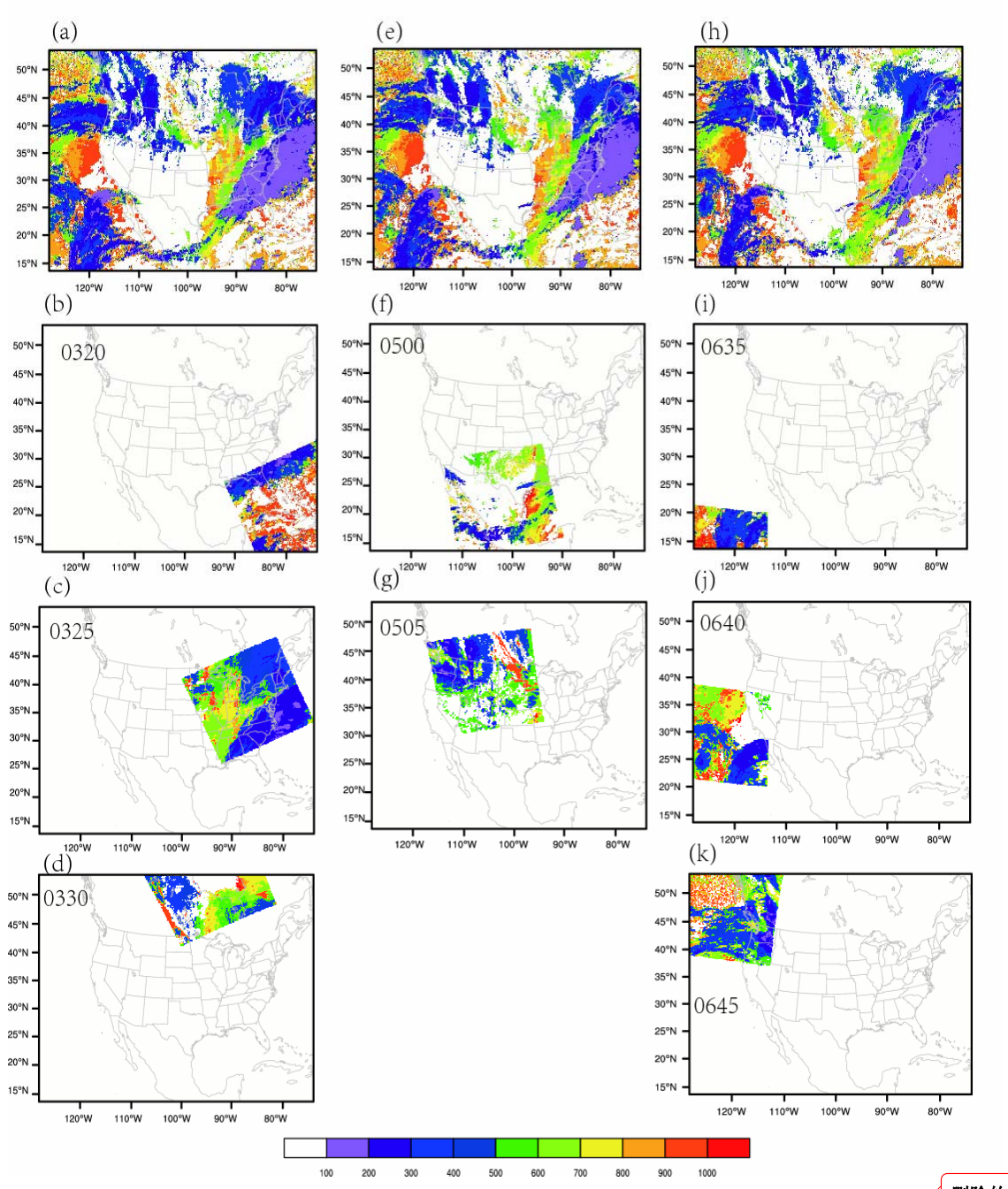

392

393 **Figure 8**. The cloud top pressure for (a) 0300UTC from the GOES NASA retrieval, (b) 0320UTC,

394 (c) 0325UTC, (d) 0330UTC from MODIS level-2 products; (e) 0500UTC from the GOES NASA

395 retrieval, (f) 0500UTC, (g) 0505UTC; (h) 0700UTC from the GOES NASA retrieval, (i)

396 0635UTC, (j) 0640UTC, and (k) 0645UTC from MODIS level-2 products.

删除的内容: 7

Fig. 9 presents the correlation coefficients and biases of the CTP and CBP verified against the NASA GOES and MODIS retrievals. The solid lines denote the results regarding the CTP and CBP versus the NASA GOES products from 0000 UTC to 0700 UTC, while the dots describe the CTP results versus the cloud top retrievals in NASA MODIS level-2 products at 0320UTC, 0325UTC, 0330UTC, 0500UTC, 0505UTC, 0635UTC, 0640UTC, and 0645UTC. Here the negative bias means that the retrieved clouds are higher than the reference. Vice versa, the positive bias indicates the clouds are put too low. We conducted another experiment "APFimg" that applies solely GOES Imager data to check the added value from the high spectral resolution radiances (such as, CrIS, AIRS, and IASI). In Fig. 9a, the correlations between the retrievals from MMR and the NASA GOES retrievals are comparable with from APF for most hours; APF gains overall higher correlations with the CTPs in the MODIS retrievals. From the bias in Fig. 9b, it seems that the CTPs from MMR are underestimated (putting the clouds too high) consistently against both retrievals with GOES and MODIS radiances. Fig. 9c shows that the correlations are weaker for MMR compared to others all the time. In Fig. 9d, the positive CBP biases from MMR are remarkable, while the CBP biases from APF are largely reduced. Generally, APFimg degrades the CTP and CBP results consistently, suggesting that radiances with high spectral resolutions are able to improve the vertical descriptions of cloud profiles. It is found that the clouds retrieved with APFg2 are shrunken in terms of cloud depth with notably lower cloud top and higher cloud base compared to APF, when excluding the perturbed particles in the first group.

删除的内容: 8

删除的内容: 8

删除的内容: 8

删除的内容: 8

删除的内容: 8

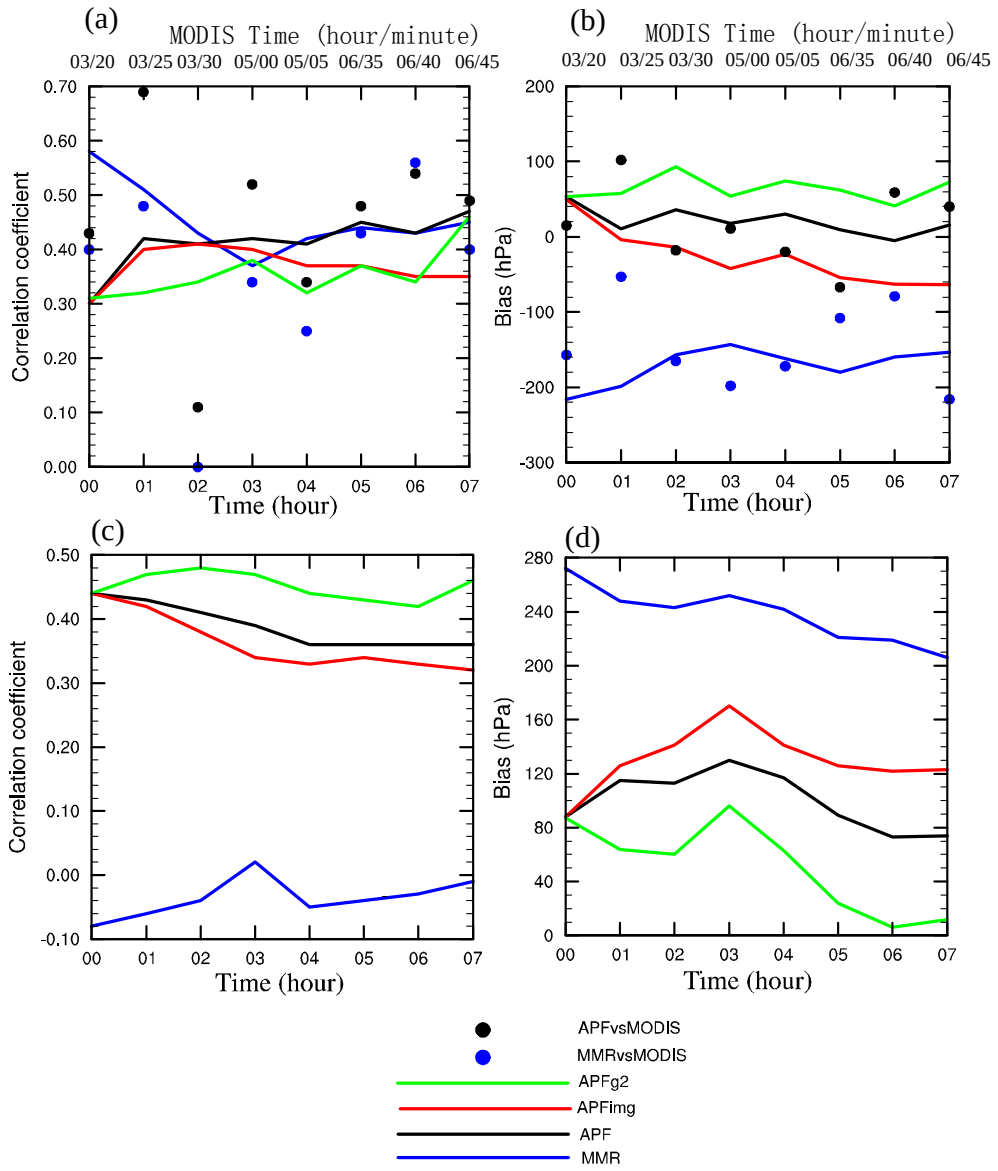

Figure 9. (a) Correlation coefficient, (b) bias for the cloud top pressure, (c) correlation coefficient, and (d) bias for the cloud bottom pressure versus the NASA GOES retrievals from 0600 UTC 15 December 2013 to 0700 UTC 15 December 2013. Black and blue dots denote results versus the MODIS level-2 cloud top pressure retrieval valid at 0320UTC, 0325UTC, 0330UTC, 0500UTC, 0505UTC, 0635UTC, 0640UTC, and 0645UTC. The valid times for the MODIS level-2 data are

删除的内容: 8

shown on the top of the x-axis.

4.5 Computational issues

Fig. 10a represents the elapsed times for the MMR and APF experiments and the counts of radiance observations in use are shown in Fig. 10b from 0000 UTC to 0700 UTC 12 December 2013. The profile of computing time in MMR is quite different from that in PF. The cost of MMR is dominated by the heavy minimization procedure, while APF is more associated with the processes of initializing particles and calculating weights for all the particles. The computing times were measured from cloud retrieving runs with 64 MPI-tasks on a single computing node in an IBM iDataPlex Cluster. The measured wall clock computing times show that generally MMR is computationally more expensive for most of the time than APF. It seems the wall clock times for MMR are generally proportional to the data amount used. While for the APF experiment, the wall clock time is mostly determined by the particles size and partly affected by the channel number, such as for 2013121202 and 2013121206, when the total counts of the hyperspectral sensors (IASI, CrIs, and AIRS) are large. The PF experiments using particles of one-layer cloud with 100% cloud fractions usually take less than 5 minutes for the same periods (not shown).

删除的内容: 9

删除的内容: 9

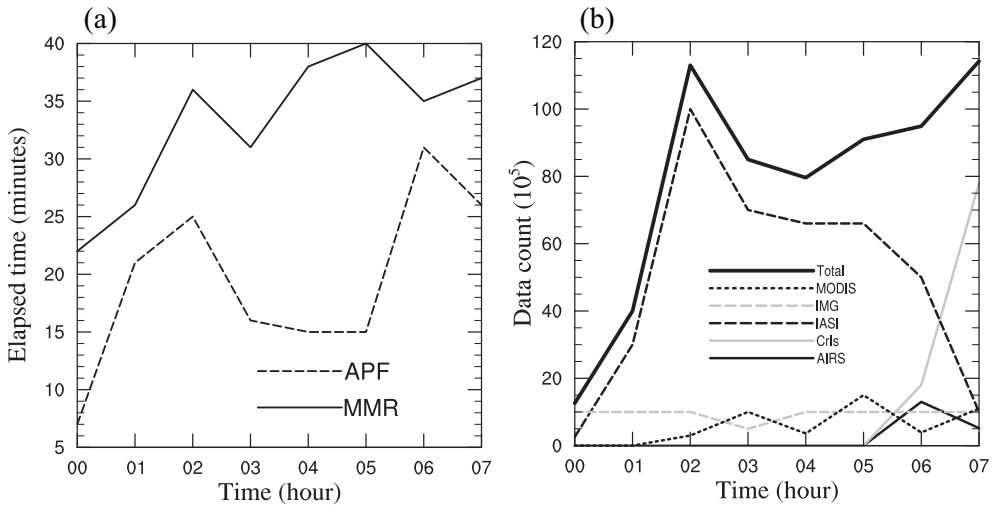

443

444 **Figure 10**. (a) The elapsed time and (b) the data count from 0000 UTC to 0700 UTC 15 December

删除的内容: 9

445 2013.

446 4.6 Resolving the filtering problem on model grids

447 As explained in subsection 3.3, the filtering problem is resolved in the radiance
448 observational space at each FOV of each sensor independently and sequentially. For
449 each FOV, the retrieved cloud fractions are extrapolated to its neighboring model grid
450 points afterwards. We order the sensors in the cloud retrieving procedure as
451 GOES-Imager, MODIS, CrIS, AIRS, and IASI, aiming to optimize the vertical clouds
452 using sensors featured with sufficient spectral resolutions. As a consequence, the
453 retrievals from the last sensor determine the final output to the most extent, causing
454 the cloud retrievals highly subjective to the ordering of the sensors. On the other hand,
455 it means the information from other prior sensors will be more or less discarded. In
456 this section, a different way of resolving the filtering problem is preliminarily tested,
457 in which the weights for each particle are aggregated over all available sensors by

calling the forward radiative transfer model on neighbouring model grids.

Fig. 11 shows the clouds retrievals from the grid-based method. It is noted that the grid-based scheme yields slightly worse results of CTP and neutral results of CBP compared with those from the observation-based (FOV-based) scheme, indicating that the hyperspectral sensors probably favor the retrieved CTP and CBP in the FOV-based scheme, which are available for most of the time. It is worth pointing out that the ordering of different sensors has nearly no effect on the final cloud retrievals, when the weights of the particles are calculated in model space (not shown). The final cloud retrieval is no longer overwritten by the retrieval from the last sensor but is a total solution with all the sensors fairly considered, instead. The computational cost of retrieving clouds in model space is comparable or slightly heavier than that in observation space. The computational cost of the grid-based scheme scales with the number of the computing nodes more directly, compared to that of the FOV-based scheme.

删除的内容: 0

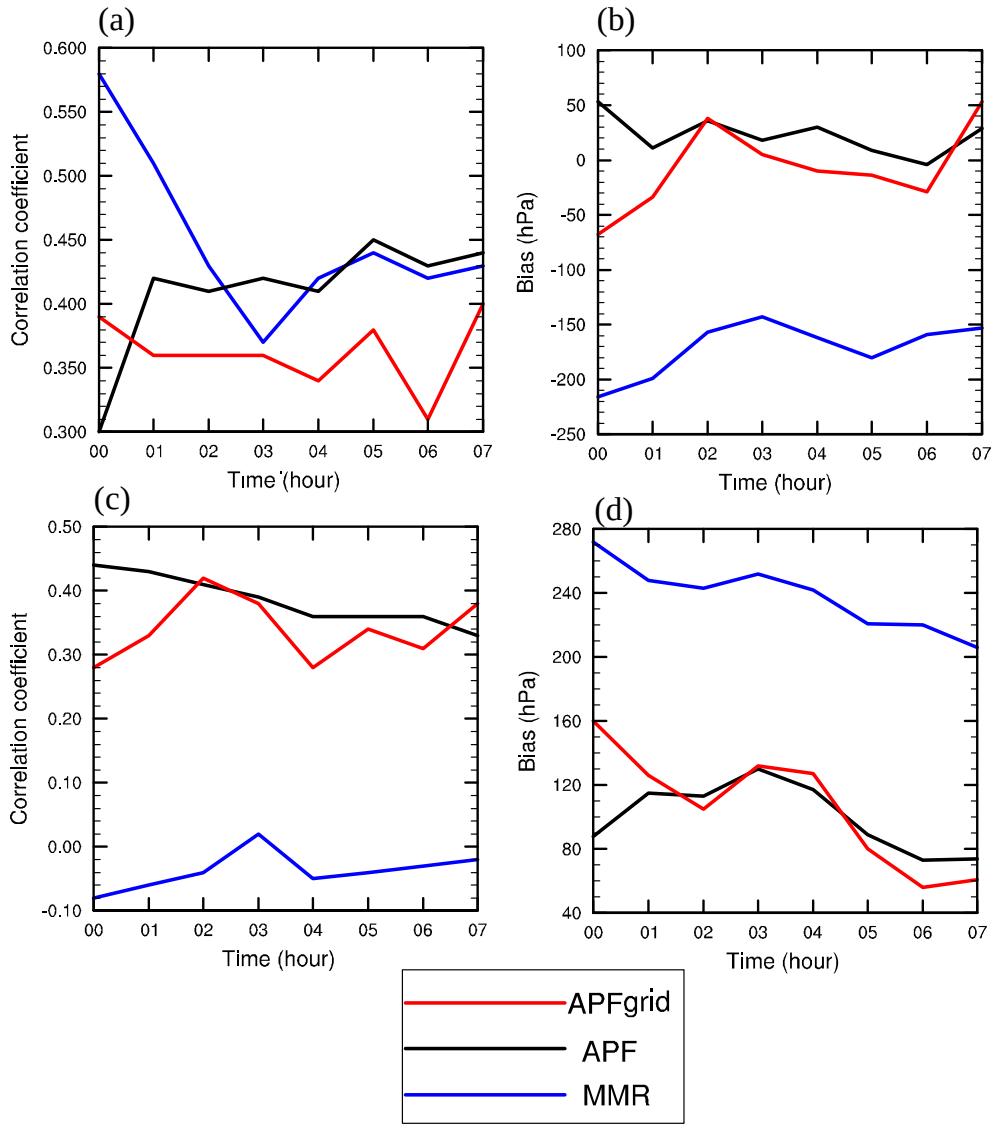

Figure 11. (a) Correlation coefficient, (b) bias for the cloud top pressure, (c) correlation coefficient, and (d) bias for the cloud bottom pressure versus the NASA GOES retrievals from 0000 UTC to 0700 UTC 15 December 2013.

删除的内容: 0

5. Discussion and conclusion

This study presents a new cloud retrieval method based on the particle filter (PF) in the framework of GSI, as a competitive alternative to the MMR method. The behaviors of different particle initializations are demonstrated on one single field of view and the CONUS domain respectively. Comparisons between the PF and the MMR method are conducted in terms of the features of cloud mask, cloud top, cloud base, and the vertical distributions of clouds. It was found that the PF method retrieves clear cloud signals while MMR is more ambiguous in detecting clouds. By adding more small-fraction particles, high clouds can be better interpreted. From the statistical results, it was found that MMR underestimates the cloud top pressures (put the clouds top too high) and overestimates the cloud bottom pressures (put the clouds top too low) as well. APF improves both the retrievals of cloud tops and cloud bases remarkably, especially for the cloud bases. As expected, radiances with high spectral resolutions contribute to quantitative cloud top and cloud base retrievals. In addition, a different way of resolving the filtering problem over each model grid is tested to aggregate the weights with all available sensors considered, which is proven to be less constrained by the ordering of sensors. Last but not least, the PF method is overall more computationally efficient; the cost of the model grid-based PF method scales more directly with the number of the computing nodes.

In future work, validation studies using multispectral imagers on geostationary satellites, spaceborne lidars (or radar), and surface site data will continue, and the results will be used to update the retrieval algorithm. Maximizing the consistency in the products across platforms and optimizing the synergistic use of multiple-source

radiances in the new algorithm are important aspects. To estimate the flow dependent uncertainties in the cloud analysis and in the forecasts, the ensemble nowcasting with three dimensional cloud fractions via the rapid-update cycling mode is also planned. Increasing the highest extent cloudy cases will be included in future studies. Finally, the use of cloud liquid water and ice mixing ratios retrieved from the cloud fractions using multi-sensor radiances to pre-process the first guess in numerical weather forecast is another promising application.

Code and/or data availability

The MMR cloud retrieval codes can be obtained freely from (http://www2.mmm.ucar.edu/wrf/users/wrfda/). The other codes can be obtained by emails from the authors.

Acknowledgments

This work was jointly sponsored by the Natural Science Foundation of Jiangsu Province under Grant No BK20160954, the 973 Program (Grant No. 2013CB430102) , the Beijige Funding from Jiangsu Research Institute of Meteorological Science (BJG201510), the National Natural Science Foundation of China (41375025), and the Priority Academic Program Development of Jiangsu Higher Education Institutions (PAPD). The authors would like to thank Chris Davis for fruitful discussions, and Bobbie Weaver for editing the manuscript. We greatly thank the anonymous reviewers for their valuable comments on the earlier versions of the manuscript.

REFERENCES

Ackerman, S. A., K. I. Strabala, W. P. Menzel, R. A. Frey, C. C. Moeller, and L. E. Gumley: Discriminating clear sky from clouds with MODIS, Geophys. Res. Atmos., 103, 32141-32157, 1998.

Auligné, T., Lorenc, A., Michel, Y., Montmerle, T., Jones, A., Hu, M., and Dudhia, J.: Toward a New Cloud Analysis and Prediction System, B Am Meteorol Soc, 92, 207-210, 2011.

Auligné, T.: Multivariate minimum residual method for cloud retrieval. Part I: Theoretical aspects and simulated observation experiments, Monthly Weather Review, 142, 4383-4398, 2014a.

Auligné, T.: Multivariate minimum residual method for cloud retrieval. Part II: Real observations experiments, Monthly Weather Review, 142, 4399-4415, 2014b.

Aumann, H. H., Chahine, M. T., Gautier, C., Goldberg, M. D., Kalnay, E., McMillin, L. M., Revercomb, H., Rosenkranz, P. W., Smith, W. L., and Staelin, D. H.: AIRS/AMSU/HSB on the Aqua mission: Design, science objectives, data products, and processing systems, Geoscience and Remote Sensing, IEEE Transactions on, 41, 253-264, 2003.

Bayler, G. M., Aune, R., and Raymond, W.: NWP cloud initialization using GOES sounder data and improved modeling of nonprecipitating clouds, Monthly weather review, 128, 3911-3920, 2000.

Berrocal, V. J., Raftery, A. E., and Gneiting, T.: Combining spatial statistical and ensemble information in probabilistic weather forecasts, Monthly Weather Review, 135, 1386-1402, 2007.

Blumstein, D., Chalon, G., Carlier, T., Buil, C., Hebert, P., Maciaszek, T., Ponce, G., Phulpin, T., Tournier, B., and Simeoni, D.: IASI instrument: Technical overview and measured performances, Optical Science and Technology, the SPIE 49th Annual Meeting, 2004, 196-207,

Brückner, M., Pospichal, B., Macke, A., and Wendisch, M.: A new multispectral cloud retrieval method for ship‐based solar transmissivity measurements, Journal of Geophysical Research: Atmospheres, 119, 2014.

Descombes, G., Auligne, T., and Lin, H.-C., Xu, D., Schwartz, C. S., Vandenberghe, F.: Multi-sensor Advection Diffusion nowCast (MADCast) for cloud analysis and short-term prediction., NCAR Technical Note NCAR/TN-509+STR, , 21 pp., 2014.

Eyre, J. R., and Menzel, W. P.: Retrieval of cloud parameters from satellite sounder data: A simulation study, Journal of Applied Meteorology, 28, 267-275, 1989.

Han, Y., Delst, P. V., Liu, Q., Weng, F., Yan, B., Treadon, R., and Derber, J.: JCSDA Community Radiative Transfer Model (CRTM)—Version 1, NOAA Tech. Rep. NESDIS, 122, 33, 2006.

Hu, M., Xue, M., and Brewster, K.: 3DVAR and Cloud Analysis with WSR-88D Level-II Data for the Prediction of the Fort Worth, Texas, Tornadic Thunderstorms. Part I: Cloud Analysis and Its Impact, Monthly Weather Review, 134, 675-698, 10.1175/mwr3092.1, 2006.

Huang, H.-L., Smith, W. L., Li, J., Antonelli, P., Wu, X., Knuteson, R. O., Huang, B.,

and Osborne, B. J.: Minimum local emissivity variance retrieval of cloud altitude and effective spectral emissivity-simulation and initial verification, Journal of applied meteorology, 43, 795-809, 2004.

Karlsson, K.-G., Johansson, E., and Devasthale, A.: Advancing the uncertainty characterisation of cloud masking in passive satellite imagery: Probabilistic formulations for NOAA AVHRR data, Remote Sensing of Environment, 158, 126-139, 2015.

Kleist, D. T., Parrish, D. F., Derber, J. C., Treadon, R., Wu, W. S., and Lord, S.: Introduction of the GSI into the NCEP Global Data Assimilation System, Weather and Forecasting, 24, 1691-1705, 10.1175/2009waf2222201.1, 2009.

Liu, Q., and Weng, F.: Advanced doubling-adding method for radiative transfer in planetary atmospheres, Journal of the atmospheric sciences, 63, 3459-3465, 2006.

Mace, G. G., 2004: Level 2 GEOPROF product process description and interface control document (v.3): Level 2 GEOPROF product process description and interface control document (v.3), Tech. rep., CIRA, Colorado State University, 2004.

Mechri, R., Ottlé, C., Pannekoucke, O., and Kallel, A.: Genetic particle filter application to land surface temperature downscaling, Journal of Geophysical Research: Atmospheres, 119, 2131-2146, 2014.

Menzel, W., Smith, W., and Stewart, T.: Improved cloud motion wind vector and altitude assignment using VAS, Journal of Climate and Applied meteorology, 22, 377-384, 1983.

Menzel, W. P., and Purdom, J. F.: Introducing GOES-I: The first of a new generation of geostationary operational environmental satellites, B Am Meteorol Soc, 75, 757-781, 1994.

Platnick, S., King, M. D., Ackerman, S. A., Menzel, W. P., Baum, B. A., Riédi, J. C., and Frey, R. A.: The MODIS cloud products: Algorithms and examples from Terra, Geoscience and Remote Sensing, IEEE Transactions on, 41, 459-473, 2003.

Rossow, W. B., and Schiffer, R. A.: ISCCP cloud data products, B Am Meteorol Soc, 72, 2-20, 1991.

Rossow, W. B., Walker, A. W., and Garder, L. C.: Comparison of ISCCP and other cloud amounts, Journal of Climate, 6, 2394-2418, 1993.

Shen, Z. Q., and Tang, Y. M.: A modified ensemble Kalman particle filter for non-Gaussian systems with nonlinear measurement functions, J Adv Model Earth Sy, 7, 50-66, 2015.

Skamarock, W., C, Klemp, J. B., Dudhia, J., Gill, D. O., Barker, D. M., Duda, G., Huang, X.-Y., Wang, W., and Powers, J. G.: A description of the Advanced Research WRF version 3., NCAR, 113, 2008.

Smith, A., Atkinson, N., Bell, W., and Doherty, A.: An initial assessment of observations from the Suomi‐NPP satellite: data from the Cross‐track Infrared Sounder (CrIS), Atmospheric Science Letters, 16, 260-266, 2015.

Snyder, C., and Zhang, F. Q.: Assimilation of simulated Doppler radar observations with an ensemble Kalman filter, Monthly Weather Review, 131, 1663-1677, Doi 10.1175//2555.1, 2003.

Stephens, G. L., Vane, D. G., Boain, R. J., Mace, G. G., Sassen, K., Wang, Z., Illingworth, A. J., O'Connor, E. J., Rossow, W. B., and Durden, S. L.: The CloudSat mission and the A-Train: A new dimension of space-based observations of clouds and precipitation, B Am Meteorol Soc, 83, 1771-1790, 2002.

van Leeuwen, P. J.: Nonlinear data assimilation in geosciences: an extremely efficient particle filter, Quarterly Journal of the Royal Meteorological Society, 136, 1991-1999, 2010.

Wu, W.-S., Purser, R. J., and Parrish, D. F.: Three-dimensional variational analysis with spatially inhomogeneous covariances, Monthly Weather Review, 130, 2905-2916, 2002.

Wu, X., and Smith, W. L.: Assimilation of ERBE data with a nonlinear programming technique to improve cloud-cover diagnostics, 120, 2009-2004, 1992.

Xu, D., Auligné, T., and Huang, X.-Y.: A Retrieval Method for 3-D Cloud Parameters Using Radiance Observations from Multiple Satellites, Advances in atmospheric physics, 32, 349-362, 2015.

Xu, D. M., Liu, Z. Q., Huang, X. Y., Min, J. Z., and Wang, H. L.: Impact of assimilating IASI radiance observations on forecasts of two tropical cyclones, Meteorology and Atmospheric Physics, 122, 1-18, 10.1007/s00703-013-0276-2, 2013.

Zhao, C., Xie, S., Klein, S. A., Protat, A., Shupe, M. D., McFarlane, S. A., Comstock, J. M., Delanoë, J., Deng, M., and Dunn, M.: Toward understanding of differences in current cloud retrievals of ARM ground‐based measurements, Journal of Geophysical Research: Atmospheres, 117, 2012.